Effect of Iron Component on the Structural Evolution of Carbon Bonds in Hydrochloric Acid-Demineralized Lignite During Pyrolysis

Yingyue Teng, Xiaoting Bian, Xiaojuan Fu, Yinmin Song,* and Xue Bai

ACCESS | Metrics & More | Article Recommendations

ABSTRACT: The pyrolysis characteristics of hydrochloric acid-demineralized Shengli lignite (SL^+) and iron-added lignite (SL^+-Fe) were investigated using a fixed-bed reactor. The primary gaseous products (CO_2, CO, H_2, and CH_4) were detected *via* gas chromatography. Fourier-transform infrared spectroscopy and X-ray photoelectron spectroscopy techniques were used to study the carbon bonding structures of the lignite and char samples. In situ diffuse reflectance infrared Fourier transform spectroscopy was used to better understand the effect of the iron component on the transformation of the carbon bonding structure of lignite. The results showed that CO_2 was released first during pyrolysis, followed by CO, H_2, and CH_4, and this order was unaffected by the addition of the iron component. However, the iron component promoted the generation of CO_2, CO (<340 °C), and H_2 (<580 °C) at lower temperatures and inhibited the formation of CO and H_2 at higher temperatures while also inhibiting the release of CH_4 throughout the pyrolysis process. The iron component may form an active complex with $C=O$ and a stable complex with $C-O$, which can promote the fracture of carboxyl functional groups and inhibit the decomposition of ether bonds, phenolic hydroxyl groups, methoxy groups, and other functional groups, thus promoting the decomposition of aromatic structures. At low temperatures, it promotes the decomposition of aliphatic functional groups and finally the bonding and fracture of functional groups in coal, leading to the change of the carbon skeleton, resulting in the change of gas products. However, it did not significantly affect the evolution of $-OH$, $C=O$, $C=C$, and $C-H$ functional groups. According to the above results, a developing reaction mechanism model of Fe-catalyzed lignite pyrolysis was established. Therefore, it is worth doing this work.
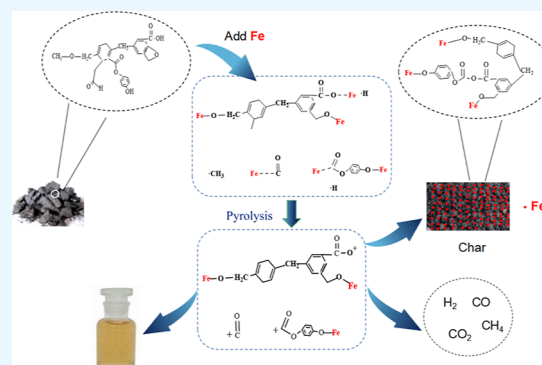
1. INTRODUCTION

Efficient utilization of low-rank coals such as lignite has attracted significant research attention.[1−4] In addition to its high water content, large amount of volatile matter, and low combustion efficiency, lignite also contains significant amounts of active organic structures and minerals.[5,6] Through pyrolysis, the water content in lignite can be removed to obtain high-added value char with improved structural properties, which improves its subsequent combustion or gasification performance. Therefore, pyrolysis is an important pathway toward efficient utilization of lignite resources.[7−9] For this reason, it is of key importance to study the pyrolysis characteristics of lignite.

The organic structure in lignite plays an important role in determining the products generated during pyrolysis.[10−13] It is believed that the distribution of pyrolysis products is related to the fracturing of bond structures, such as $C_{al}-O$, $C_{al}-C_{al}$, $C_{ar}-O$, and $C_{ar}-C_{al}$ (al: aliphatic and ar: aromatic), as well as to the polycondensation of aromatics. However, the yield and composition of pyrolysis gases are affected by the bond dissociation of carbon in carbonyl and aliphatic groups.[14,15] It has been shown that the mineral components in lignite can increase the degree of disorder of aromatic structures,[16,17]

promote the condensation of aromatic ring clusters, and inhibit the development of side chains,[2] which improve the pyrolytic properties of lignite, promote the generation of pyrolysis gases, and change the yield of tar.[18−21] The catalytic effect of the iron component has also been found to be significant[22] and is associated with the evolution of carbon bonds, which helps to improve the pyrolysis conversion rate of lignite and effectively regulates the distribution and composition of pyrolysis products. However, owing to the complex nature of different structural components of lignite, the mechanism by which the iron component affects the conversion properties of lignite during pyrolysis is not well understood. Jiang[23] found that the iron component inhibited the polymerization of char, reduced the heating value of the pyrolysis gases, and increased the yield of tar.

Gong et al.[20] put forward that the catalytic pyrolysis of the iron component improves the combustion reaction performance of lignite, changes the structure of the produced char, and promotes the formation of free radicals. Fu et al.[24] suggested that the iron component noticeably increases the yield of pyrolysis gases and char and reduces the bond energy of oxygen-containing functional groups. Their results also indicated that the iron component promotes the decomposition and hydrogenation of long chains and the dissociation of hydrogen-containing compounds, thereby further improving the reaction performance. Wang et al.[25] found that the iron component facilitated the transfer of aromatic hydrogen and that the catalytic effect of $FeCl_3$ was stronger than that of $Fe(NO_3)_3$.

The largest lignite field in China is the Shengli coal field in Inner Mongolia, which possesses more than 22.4 billion tons of lignite reserves. The efficient utilization of Shengli lignite (SL^+) is therefore of great significance to the economic development of Inner Mongolia.[26] Therefore, in order to study the influence of iron components on the evolution characteristics of the carbon bonding structure during lignite pyrolysis, this paper selects hydrochloric acid-demineralized SL^+ and iron-added lignite (SL^+-Fe) as experimental samples. The formation of pyrolysis gas of lignite was investigated by a fixed-bed device and online gas chromatography (GC). The change of functional groups during pyrolysis was studied by in situ infrared analysis. Fourier-transform infrared (FTIR) spectroscopy and X-ray photoelectron spectroscopy (XPS) were used to investigate the bonding of carbon elements during lignite pyrolysis.

2. EXPERIMENTAL SECTION

2.1. Preparation of Coal Samples. Lignite from no. 4 mine in the Shengli coal field of Inner Mongolia was selected as the experimental sample. Raw lignite with particle sizes in the range of 0.18−0.42 mm was dried at 105 °C for 4 h. The resulting sample, labeled as SL, was pretreated via a solution method[27,28] to avoid interference from the active minerals in lignite, as follows: first, SL was mixed with hydrochloric acid (18%) at room temperature in a ratio of 1 g:10 mL. After stirring for 24 h at 100 rpm, the mixture was filtered, and the filter cake was washed with water until the filtrate contained no Cl^- ions ($AgNO_3$ test) and dried at 105 °C for 4 h to obtain the hydrochloric acid-demineralized lignite sample, labeled as SL^+. Proximate and ultimate analyses were carried out on SL and SL^+ according to GB/T212-2008 using an industrial coal analyzer (China 5E-MF 6200, China) and an elemental analyzer (Vario EL Cube, Elementar, Germany), with the results shown elsewhere.[29]

Full contact between the catalyst and the coal sample was achieved via blending and impregnation methods using soluble transition-metal salts. It is generally believed that the impregnation method can infiltrate transition-metal ions into the voids of pulverized coal to maximize the effectiveness of the catalyst.[20] Therefore, iron component-added SL^+ was prepared using an impregnation method from the literature,[11,24] as illustrated in Figure 1. Based on a 5.0% iron content accounting for the mass percent of the coal sample, $FeCl_3 \cdot 6H_2O$ was dissolved in water and mixed with SL^+ while stirring for 12 h. The mixture was then dried at 105 °C for 24 h and labeled as SL^+-Fe. As shown in Table 1, X-ray fluorescence spectroscopy (ZSXPrimusII, Rigaku, Japan) showed that the SL^+ contained 3.5% iron component. Therefore, compared with the amount blended, the iron content obtained via impregnation was lower than that expected. However, this did not significantly impact

FeCl$_3$·6H$_2$O / Deionized water=1 g:10 ml

Figure 1. Diagram illustrating the impregnation method.

the study of the pyrolysis process. Proximate and ultimate analyses of the SL^+-Fe samples were also carried out according to GB/T212-2008. The results of the samples described elsewhere[29] indicate that 35.23% of ash in SL was removed by hydrochloric acid, and the ash content increased by 9.56% after adding the iron component, confirming its successful loading via impregnation.

2.2. Pyrolysis Experiments. The pyrolysis of SL^+ and SL^+-Fe was carried out in a fixed-bed reactor under an argon atmosphere, as shown in Figure 2. The mass of the coal samples used in the pyrolysis experiments was 1.5−2 g. Other parameters were as follows: a final pyrolysis temperature of 900 °C, a heating rate of 4 °C/min, a holding time of 90 min, and an argon flow rate of 200 mL/min. The resulting pyrolysis char products were labeled as SL^+-900 and SL^+-Fe-900, respectively. The char yield (Y_{char}), along with proximate and ultimate analyses of the char, is given in Table 2. The tar byproduct was condensed in cold water, while the pyrolysis gas was condensed and analyzed via GC. The working conditions of GC were set according to the retention time of the pyrolysis gas, as follows: TCD detector, a cylinder temperature of 160 °C, a sampler temperature of 180 °C, a hotwire temperature of 200 °C, and a gas collection interval of 7 min.

2.3. FTIR Spectroscopy. The organic functional groups of the lignite and char samples were analyzed using a NEXUS 6700 (Nicolet, USA) FTIR spectrometer, with a wavenumber range of 4000−400 cm^{-1} and a resolution of 4 cm^{-1}. The sample and KBr were dried at 105 °C for 4 h. The sample and KBr were mixed and ground in a ratio of 1:200, pressed, and then scanned in the IR spectrometer.

2.4. In Situ Infrared Pyrolysis Experiments. In order to further explore the influence of the iron component on the structural evolution of carbon bonding during the pyrolysis of lignite, changes in the functional groups of lignite were investigated using an IRTracer-100 (Shimadzu, Japan) in situ diffuse reflectance infrared Fourier transform spectrometer. The lignite sample was placed in the sample holder, and 15 mL/min nitrogen gas was introduced into the reaction cell for pyrolysis experiments to determine the infrared spectrum of the lignite sample. The experimental temperature ranged from 20 to 750 °C (the maximum temperature of the reaction cell) at a heating rate of 4 °C/min, a scan number of 5, and a wavenumber range of 600−4000 cm^{-1}. Starting from 150 °C, 11 temperature points were measured for every 50 °C temperature increment. Samples were directly ground and evenly put into the in situ infrared tank, in order to avoid the influence of KBr on sample pyrolysis at high temperatures.

2.5. XPS Analysis. The surface element compositions of the lignite and char samples were characterized using an ESCALAB-250Xi (Thermo Fisher Scientific, USA) X-ray photoelectron

Table 1. Mineral Composition of Ash (wt %)

sample	Na_2O	MgO	Al_2O_3	SiO_2	SO_3	Cl	CaO	TiO_2	Fe_2O_3	others
SL	2.02	5.29	18.8	36.8	16.0	1.07	10.7	0.67	5.98	2.70
SL$^+$	4.51	1.02	21.6	59.6	4.46	2.27	0.79	0.84	4.04	0.88
SL$^+$-Fe	3.94	0.83	13.5	27.8	2.51	1.24	0.83		47.2	2.23
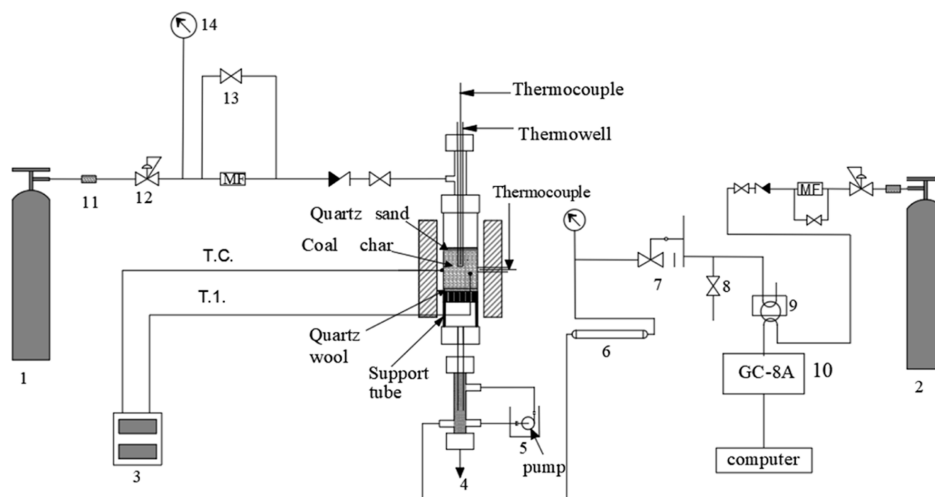
Figure 2. Schematic diagram of the fixed-bed GC experimental apparatus. (1) Reaction carrier gas; (2) chromatographic carrier gas; (3) T.C. controllers; (4) condenser/liquid−gas separator; (5) ice water; (6) cleaner; (7) back-pressure valve; (8) vent; (9) six-way valve; (10) gas chromatograph; (11) filter; (12) pressure regulator; (13) gate valve; and (14) pressure gauge.

Table 2. Yield, Proximate Analysis, and Ultimate Analysis of Pyrolysis Char Products[a]

		proximate analysis (wt %)				ultimate analysis (wt %)				
sample	yield of char (%)	M_{ad}	A_d	V_d	FC_d	C	H	N	S	O*
SL$^+$-900	60.0	1.36	18.7	5.69	75.6	70.5	1.49	0.45	1.06	7.81
SL$^+$-Fe-900	62.9	1.07	24.3	7.24	68.4	71.3	1.48	0.76	1.92	0.21

[a]A—ash content; V—volatile content; FC—fixed carbon; d—dried basis; *—by difference.
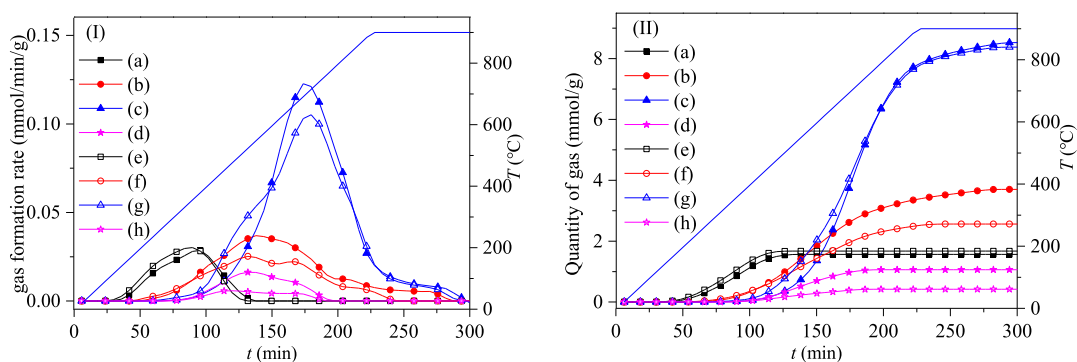
Figure 3. Release rate (I) and cumulative (II) curves of pyrolysis gases during the pyrolysis process. (a) CO_2 (SL$^+$), (b) CO (SL$^+$), (c) H_2 (SL$^+$), (d) CH_4 (SL$^+$); (e) CO_2 (SL$^+$-Fe), (f) CO (SL$^+$-Fe), (g) H_2 (SL$^+$-Fe), and (h) CH_4 (SL$^+$-Fe).

spectrometer. The XPS C 1s spectrum was peak-fitted using the Avantage software from Thermo Fisher.

3. RESULTS AND DISCUSSION

3.1. Basic Characteristics of Pyrolysis Gas Generation.
Figure 3 shows the generation rates and cumulative amounts of the four main pyrolysis gases (CO_2, CO, H_2, and CH_4). The results show that the CO_2 gas is generated first, followed by CO, H_2, and CH_4, and that the addition of the Fe component does not change the pyrolysis gas generation sequence. The characteristic temperatures and amounts of gas accumulated

Table 3. Generation Temperatures and Amounts of Pyrolysis Gases during the Pyrolysis Process

	SL$^+$		SL$^+$-Fe	
pyrolysis gases	initial temp. (°C)	cumulate (mmol/g)	initial temp. (°C)	cumulate (mmol/g)
CO_2	116	1.6	116	1.7
CO	212	3.7	189	2.6
H_2	260	8.5	236	8.4
CH_4	284	1.1	284	0.4
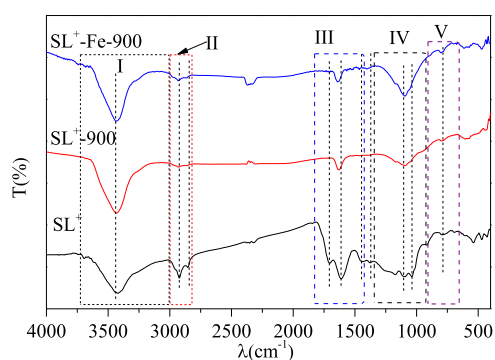
Figure 4. FTIR spectra of lignite and char samples.

during pyrolysis gas generation are listed in Table 3. From Figure 3 and Table 3, it is evident that in the initial stage of lignite pyrolysis, CO_2 is the main component of the pyrolysis gas and is mainly generated through the breaking of the carboxyl functional group.[32−34] After adding the Fe component, the CO_2 temperature zone for generation is shortened and its rate of formation is increased significantly. As a result, the gas accumulation is increased by 7.1%, indicating that the complexation of the Fe component with the carboxyl group facilitates its rupture, thereby promoting CO_2 generation.

During lignite pyrolysis, CO is mainly generated through the breaking of functional groups such as aldehyde, carbonyl, phenolic hydroxyl, and ether.[28,32] At low temperatures, CO is generated *via* aldehyde group decomposition, while at high temperatures, it is mainly derived from the decomposition of methoxy groups, secondary reactions of tar (involving the breakage of the ether bonds connecting the aromatic rings), and the breakage of ethers, hydroxyl groups, and oxygen-containing heterocyclic structures. After adding the Fe component, the CO generation temperature and the gas accumulation both decreases, the latter by 30.8%. At pyrolysis temperatures <340 °C, the CO generation rate increases, indicating that the Fe component promotes the decomposition of aldehyde groups at this stage. However, when the pyrolysis temperature is >340 °C, the CO generation rate decreases, indicating that the Fe component inhibits the decomposition of functional groups such as ether, phenolic hydroxyl, and methoxy, as well as the secondary reaction of tar.

Hydrogen is generally considered to be a secondary pyrolysis product of lignite and is mainly derived from the polymerization of aromatic substances and the high-temperature dehydrogenation of aromatic rings.[32−34] After adding the Fe component, the generation temperature of H_2 and the gas accumulation both decreases, the latter by 1.7%. When the pyrolysis temperature is <580 °C, the generation rate of H_2 increases significantly, indicating that the Fe component promotes the decomposition of aromatic structures,[35,36] resulting in the breakage of the aliphatic side chains connected to it and the removal of large numbers of hydrogen radicals. These results are consistent with those of Fu.[20] When the pyrolysis temperature is >580 °C, the rate of generation of H_2 decreases, indicating that the Fe component inhibits further polymerization of free radicals[27] and therefore the generation of H_2, by inhibiting the breakage of oxygen-containing heterocyclic rings and the condensation of phenolic hydroxyl groups and agglomerates on the carbon surface.[28]

During the pyrolysis of lignite, CH_4 mainly originates from the pyrolysis of methoxy groups and the breakage of aliphatic side chains in the lignite (at low temperatures) and the breakage of aromatic side chains (at high temperatures).[28,33] After adding the Fe component, the formation rate of CH_4 and the gas accumulation both decreased, the latter by 60.5%, indicating that the Fe component suppresses the pyrolysis of methoxy groups, aliphatic side chains, and aromatic side chains.

3.2. Functional Group Analysis. Figure 4 shows the FTIR spectra of the lignite and char samples. As the figure shows, the FTIR spectra of the lignite and char samples were classified into five sections as follows: 3675−3000 cm^{-1} (I), 2990−2800 cm^{-1} (II), 1780−1410 cm^{-1} (III), 1340−900 cm^{-1}(IV), and 900−650 cm^{-1}(V).[36−38] Differences between the FTIR spectra of the SL^+ and char samples can be clearly observed in Figure 4.[39,40] In Section I (3675−3000 cm^{-1}), the peak around 3426 cm^{-1} is the hydroxyl (−OH) bond absorption peak. The effect of iron composition on the −OH group cannot be accurately judged, as FTIR does not completely guarantee the absence of moisture. In Section II, 2935 and 2859 cm^{-1} are C−H characteristic peaks; the intensity of the aliphatic C−H characteristic peak of the chars is significantly weakened, with that of SL^+-Fe-900 being slightly stronger, which indicates that the Fe component reduces the amount of aliphatic functional groups' decomposition during pyrolysis to a certain extent. This is consistent with the CH_4 generation data seen earlier. In Section III, C=O characteristic
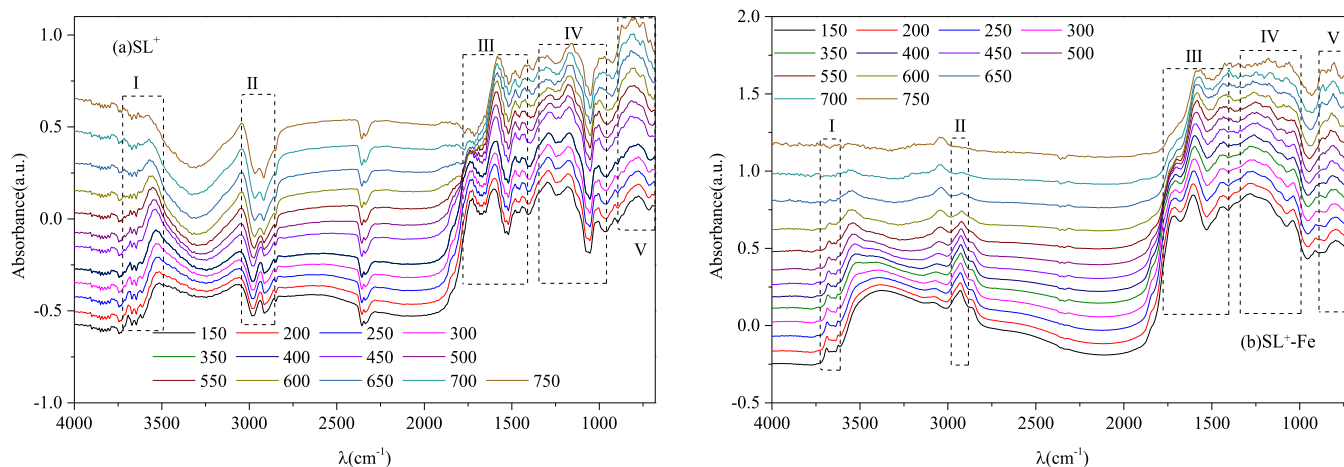
Figure 5. DRIFTS spectra of lignite samples pyrolyzed at different temperatures.

Table 4. Fitted DRIFTS Peak Classification of the Lignite Samples

figure	peak	center (cm^{-1})	group	assignment
(a)	1	3713.2	O−H	stretching vibration of O−H in clay mineral
	2	3700.7	O−H	stretching vibration of O−H in clay mineral
	3	3692.2	O−H	stretching vibration of O−H in clay mineral
	4	3681.6	O−H	stretching vibration of O−H in clay mineral
	5	3661.4	O−H	stretching vibration of O−H in clay mineral
	6	3656.2	O−H	stretching vibration of O−H in clay mineral
	7	3637.0	O−H	stretching vibration of O−H in clay mineral
	8	3627.1	O−H	stretching vibration of O−H in clay mineral
	9	3621.7	O−H	stretching vibration of O−H in clay mineral
	10	3597.6	O−H	stretching vibration of O−H in clay mineral
	11	3586.5	O−H	stretching vibration of O−H in clay mineral
(b)	12	2952.0	−CH$_3$	asymmetric stretching vibration of CH$_3$
	13	2935.2	−CH$_2$	asymmetric stretching vibration of CH$_2$ in alkanes
	14	2864.5	−CH$_3$	symmetric stretching vibration of CH$_3$
	15	2833.9	−CH$_2$	symmetric stretching vibration of CH$_2$ in alkanes
	16	2812.8	−CH$_2$	symmetric stretching vibration of CH$_2$ in alkanes
(c)	17	1757.9	C═O	stretching vibration of C═O; monomer RCOOH
	18	1729.2	C═O	stretching vibration of C═O in conjugated esters; aromatic fat; aromatic ketone; aromatic free acid; monomer CH$_2$═CH−COOH
	19	1697.1	C═O	stretching vibration of C═O in carboxylic acids; aromatic aldehyde; CH$_2$═CH−COOH═CH−COOH; C═C−CHO; ArRC═O
	20	1661.9	C═O	stretching vibration of highly conjugated C═O; C═C−C(R)═O
	21	1623.7	C═C	stretching vibration of C═C in aromatic rings
	22	1591.9	C═C	stretching vibration of C═C in aromatic rings
	23	1564.9	C═C	stretching vibration of C═C in aromatic rings; asymmetric stretching vibration of COO in carboxylates
	24	1486.4	C═C	stretching vibration of C═C in aromatic rings
	25	1440.6	−CH$_3$	asymmetric deformation vibration of CH$_3$
(d)	26	1303.4	C−O	asymmetric stretching vibration of C−O−C in cyclic ethers
	27	1272.9	C−OH	stretching vibration of C−OH in phenols
	28	1235.1	C−O	asymmetric stretching vibration of C−O−C in aliphatic ethers
	29	1203.0	C−O	asymmetric stretching vibration of C−O−C in aromatic ethers
	30	1173.5	C−OH	stretching vibration of C−OH in phenols
	31	1144.8	C−OH	stretching vibration of C−OH in phenols
	32	1109.3	Si−O	stretching vibration of Si−O in aluminosilicates
	33	1025.8	Si−O	stretching vibration of Si−O in aluminosilicates
	34	1005.9	Si−O	stretching vibration of Si−O in aluminosilicates
(e)	35	870.2	═C−H	out-of-plane deformation vibration of ═C−H in aromatic structures with isolated aromatic hydrogens (1H)
	36	842.4	═C−H	out-of-plane deformation vibration of ═C−H in aromatic structures with two adjacent hydrogens per ring (2H)
	37	819.7	═C−H	out-of-plane deformation vibration of ═C−H in aromatic structures with two adjacent hydrogens per ring (2H)
	38	795.3	═C−H	out-of-plane deformation vibration of ═C−H in aromatic structures with three adjacent hydrogens per ring (3H); symmetric stretching vibration of amorphous silicon and amorphous silicon
	39	771.8	═C−H	out-of-plane deformation vibration of ═C−H in aromatic structures with three adjacent hydrogens per ring (3H)
	40	747.6	═C−H	out-of-plane deformation vibration of ═C−H in aromatic structures with four adjacent hydrogens per ring (4H)
	41	695.1	═C−H	stretching vibration of Si−O−Al in aluminosilicates; out-of-plane deformation vibration of ═C−H in aromatic structures with five adjacent hydrogens per ring (5H)

peaks at 1707 cm^{-1} and aromatic C═C characteristic peaks at 1610 cm^{-1} are mainly present; the intensity of the characteristic peaks corresponding to the C═O functional group decreases, indicating that C═O is easily decomposed during pyrolysis. The iron component showed no obvious effect on the changes in these functional groups. In Section IV, the characteristic peaks are at 1000−1300 cm^{-1} of oxygen-containing functional groups such as alcohols, phenols, ethers, and/or esters, and their intensity decreases. The intensity of the characteristic peaks corresponding to the functional groups of the chars is reduced. In particular, the intensity of the characteristic peaks of SL$^+$-Fe-900 is relatively enhanced in the range of 1300−1000 cm^{-1}, indicating that the iron component inhibits the decomposition of C−O to some extent. This is consistent with the amount of CO released in the high-temperature stage (>340 °C). In the

fifth part (Section V), the iron component showed no obvious effect on the variation of aromatic C−H bonds.

3.3. Functional Group Evolution during Pyrolysis.
Figure 5 shows the pyrolysis diffuse reflectance infrared Fourier transform spectroscopy (DRIFTS) spectra of the two lignite samples at different temperatures, and the organic functional groups are same as those observed in the FTIR spectra in Figure 4. According to the relevant literature,[30,31] the measurement range can be divided into five distinct regions (labeled 1−5), same as the infrared partition method. Figure 5 also shows that there are three main types of organic functional groups present in the lignite and char samples, namely aliphatic structures, aromatic structures, and oxygen-containing functional groups.[37] As the temperature increases, hydroxyl (−OH) absorption peaks appear in the spectrum, and the intensity of the
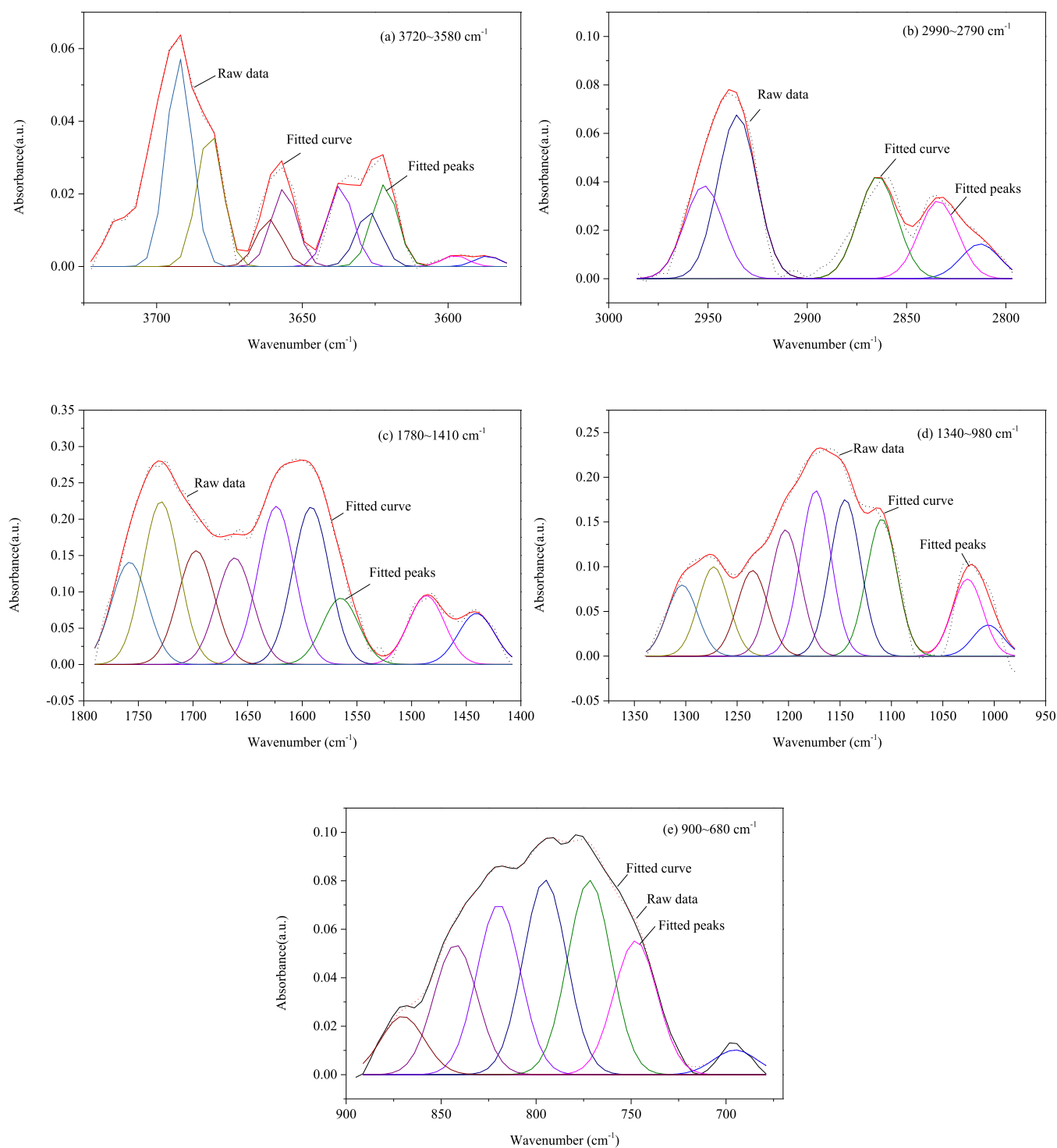
Figure 6. Fitted DRIFTS curves for SL$^+$ at 150 °C.

characteristic peaks decreases in region 1 (3580−3720 cm^{-1}). The aliphatic C−H structure, the characteristic peak of the C=O functional group, and the intensity of the C−O characteristic peaks in region 2 (2800−990 cm^{-1}), region 3 (1410−1780 cm^{-1}), and region 4 (980−1340 cm^{-1}) were significantly decreased, which were the same as the FTIR results. The intensity of the characteristic peaks of C−H functional groups in region 5 (680−900 cm^{-1}) is not obvious. Compared with FTIR, DRIFTS can better show the changes of functional groups in the pyrolysis process.

To further semi-quantitatively study the changes in functional groups, curve fitting analysis was performed on the DRIFTS spectra of lignite samples at different temperatures using a peak fitting software, with the results shown in Table 4. According to a method from the literature,[30] the infrared spectra of the samples were divided into five wavenumber segments. As an example, Figure 6 shows the SL$^+$ spectrum at 150 °C. Figure 7 shows the functional group content of lignite samples at different temperatures, calculated as follows
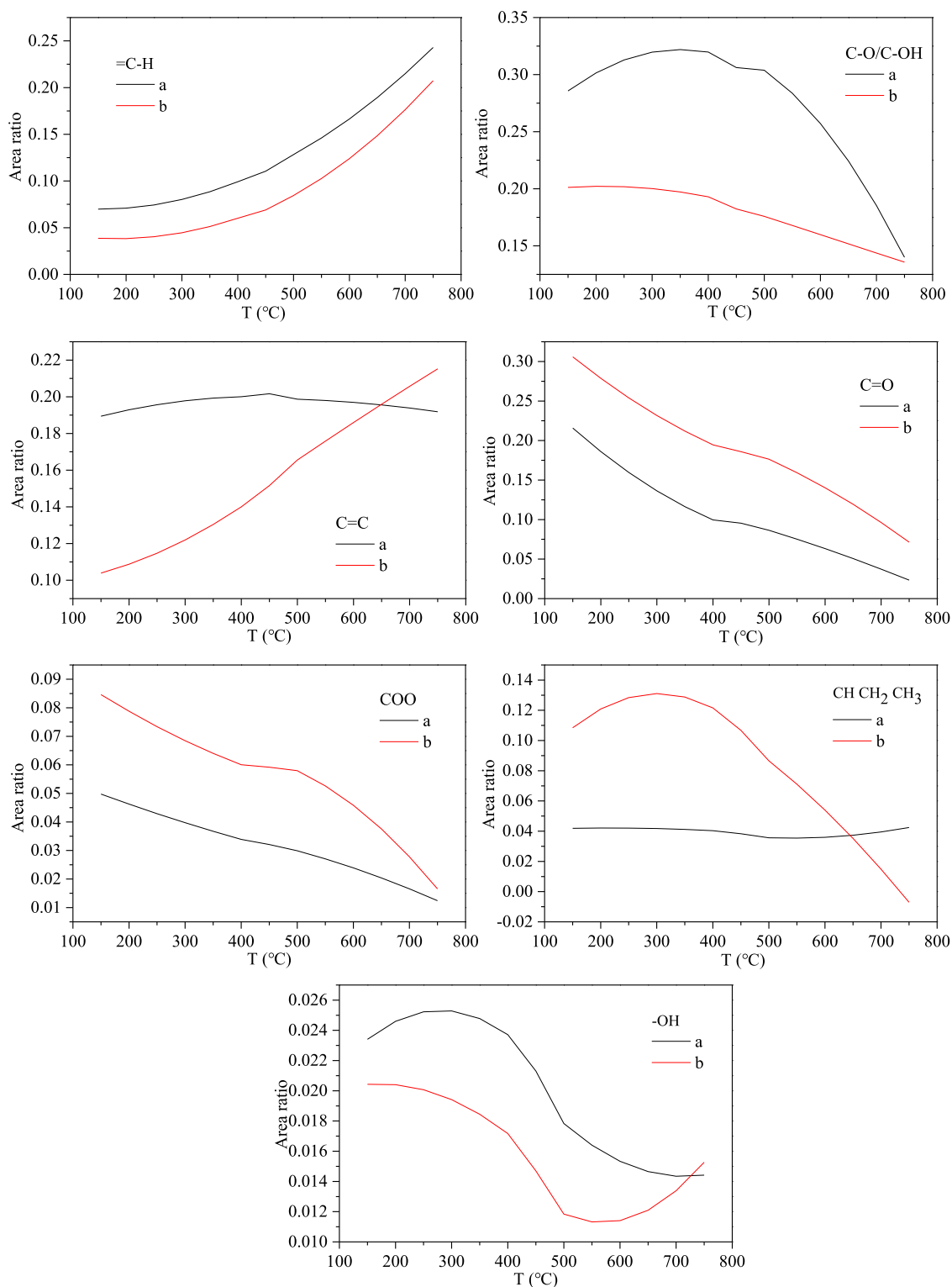
Figure 7. Functional group content of lignite samples at different temperatures: (a) SL$^+$ and (b) SL$^+$-Fe.

$$A_\chi / A_{\text{total}} \qquad (1)$$

where A is the peak area and the subscript χ can refer to either aromatic C−H, C−O/C−OH, C═C, C═O, aliphatic C−H, or free −OH structures.

Figure 7 is the fitting result of in situ DRIFTS spectra at different temperatures. As lignite pyrolysis gas completely escaped before 900 °C, the maximum upper limit temperature

of DRIFTS is 750 °C. Figure 7 shows that as the pyrolysis temperature increased, the aromatic C−H bond content in SL$^+$ increased, indicating that the related functional groups underwent pyrolysis or condensation reactions. This is consistent with the removal of the aromatic side chains to a certain extent, resulting in an increase in the number of aromatic C−H bonds. On the other hand, the contents of free C−O/C−OH, C═O, and −OH structures decreased, indicating that the oxygen-
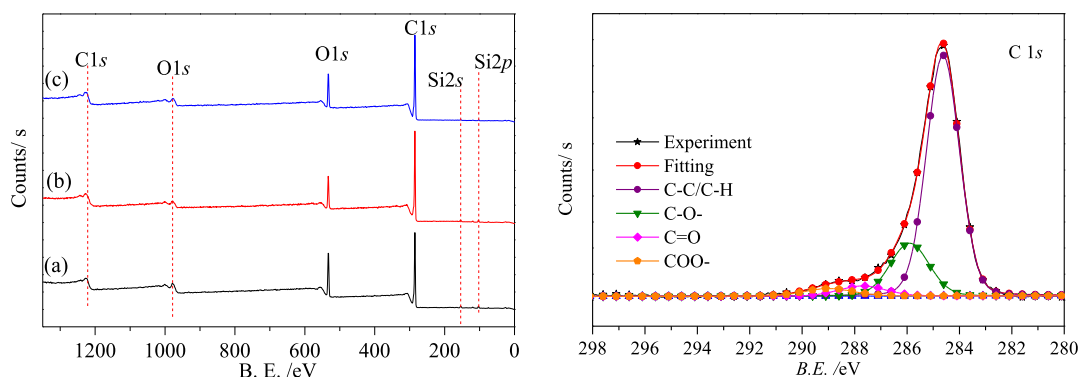
Figure 8. XPS and C 1s fitted curves of lignite and char samples: (a) SL$^+$, (b) SL$^+$-900, and (c) SL$^+$-Fe-900.

Table 5. XPS C 1s Fitting Data of Lignite and Char Samples

samples	content (%)			
	C−C/C−H	C−O/C−OH	C=O	COO−
SL$^+$	76.5	11.8	4.03	7.73
SL$^+$-900	86.3	6.24	2.48	4.96
SL$^+$-Fe-900	73.4	20.2	3.94	2.41

containing functional groups in lignite are easily decomposed. By contrast, the C=C bonds in aromatic hydrocarbons were relatively stable, indicating that the carbon skeleton of the lignite barely changed. The iron component also had no obvious effect on the aliphatic C−H, −OH, and C=O conversions in the aromatic structures. After adding the iron component, however, the amount of aromatic C−H bonds decreased, indicating that the Fe component inhibits the polymerization of aromatic structures, which is consistent with the H$_2$ generation results seen earlier. The contents of C−O/C−OH and −OH bonds were also reduced in the presence of the Fe component, indicating that it has an inhibitory effect on the decomposition of

functional groups such as ether bonds, phenolic hydroxyl groups, and methoxy groups. This result is consistent with the generation of H$_2$, CO, and CH$_4$. The Fe component also increases the C=O and COO contents of the lignite sample, while the rate of decomposition of COO increases. This demonstrates that the complexation of the Fe component with carboxyl groups facilitates the rupture of these groups, which is consistent with the CO$_2$ generation results. Additionally, the Fe component increases the content and the rate of decomposition of aliphatic C−H bonds, indicating that it promotes the formation of free aliphatic groups while promoting the decomposition of aliphatic functional groups. The aromatic C=C bonds in SL$^+$-Fe decreased significantly, and the C=C bonds increased with increasing temperature, which could be due to changes in the carbon skeleton caused by the formation and rupture of functional groups.

3.4. Analysis of Carbon Element Bonding Structure. Figure 8 shows the XPS C 1s fitting results of the lignite and char samples; hence, it can be seen that the carbon element bonding structures can be classified into four types: aromatic units and
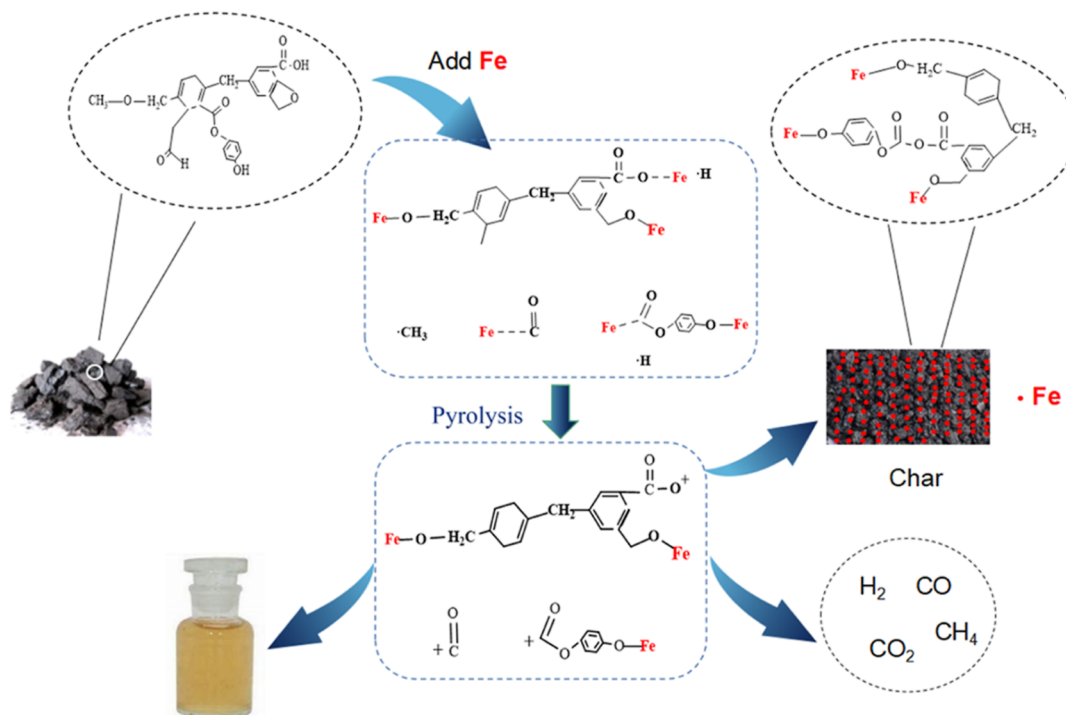
Figure 9. Reaction mechanism of iron-catalyzed lignite pyrolysis.

their substituents (C−C/C−H, 284.8 eV), ether or phenolic hydroxyl groups (C−O/C−OH, 286.1 eV), carbonyl groups (C=O, 287.6 eV), and carboxyl bonds (COO−, 289.0 eV),[11,41] where C−C and C−H are the main bonding forms of the carbon element. The results show that the four functional groups still exist after pyrolysis of SL[+]-Fe. The XPS C 1s fitting parameters of the samples are listed in Table 5. Table 5 shows that within the experimental temperature range, the content of C−C/C−H structures in the lignite increased and that of C=O structures decreased, consistent with the results of FTIR. After adding the Fe component, the C−C/C−H content of the char samples decreased, the C−O/C−OH content increased significantly, the C=O content increased only slightly, and the content of the COO− structure decreased. In conjunction with the DRIFTS results, it is evident that the iron component promotes the fracture of the C−C/C−H structures during pyrolysis, which may be due to the formation and dissociation of bonds between the iron component and the organic structure, leading to changes in the carbon skeleton. This is consistent with the generation of H_2 in the low-temperature stage (<580 °C). The Fe component inhibits the decomposition of phenolic hydroxyl groups, ether bonds, and methoxy groups and may form stable organic salts containing the C−O structure, to increase its content, which is consistent with the generation of CO and CH_4. Simultaneously, the presence of iron component may result in the formation of active C=O−Fe, COO−Fe, or Fe−COO, Fe−C=O organic salts with C=O and COO− structures, which promotes the dissociation of aldehyde groups and carboxyl groups, thus increasing the content of C=O and decreasing the content of COO. This result is consistent with the FTIR and CO_2 generation results seen earlier.

3.5. Mechanism of Iron Component-Catalyzed Lignite Pyrolysis. During the pyrolysis of lignite, the formation of iron-containing organic salts can promote the cleavage of aliphatic side chains and aromatic rings containing aldehydes or esters and inhibit the dissociation of oxygen-containing heterocycles, ethers, and phenolic hydroxyl aromatic rings. As discussed in Section 2.1, the Fe component promotes the formation of CO_2, CO (<340 °C), and H_2 (<580 °C) and inhibits the formation of CH_4. A combination of FTIR and XPS structural characterization showed that the aromatic macromolecular system of carbon was destroyed, resulting in changes in the produced gases. The formation and dissociation of bonds between the Fe component and the organic structures led to changes in the carbon skeleton. Due to the changes in oxygen-containing structures such as aldehyde and ester groups in the aromatic ring side chains, oxygen-containing active free radicals and aliphatic side chains were obtained, facilitating the easy escape of CO_2, CO, and H_2 and hindering that of CH_4. The oxygen-containing radicals reform carbon-containing organic substances when they encounter stable carbon structures, forming char. The reaction mechanism of Fe-catalyzed lignite pyrolysis is illustrated in Figure 9.

4. CONCLUSIONS

In this paper, the effect of $FeCl_3$ on the evolutionary characteristics and carbon structure of lignite pyrolysis gas was investigated. The results show that the Fe component in lignite changes the reaction pathway of oxygen-containing functional groups in lignite, thus changing the distribution of pyrolysis products and significantly affecting the structure of aromatic rings in semi-coke samples. More carbon−oxygen bonds (single and double bonds) were retained in the final char. In contrast,

the contents of C−C/C−H, carboxyl, and ester structures were reduced.

■ AUTHOR INFORMATION

Corresponding Author

Yinmin Song − *College of Chemical Engineering, Inner Mongolia Key Laboratory of High-Value Functional Utilization of Low Rank Carbon Resources, Inner Mongolia University of Technology, Hohhot, Inner Mongolia 010051, China; Experimental Management Center (Testing Center), Inner Mongolia University of Technology, Hohhot, Inner Mongolia 010051, China;* orcid.org/0000-0003-0667-7760; Phone: +86 18947198211; Email: songyinmin@imut.edu.cn

Authors

Yingyue Teng − *College of Chemical Engineering, Inner Mongolia Key Laboratory of High-Value Functional Utilization of Low Rank Carbon Resources, Inner Mongolia University of Technology, Hohhot, Inner Mongolia 010051, China;* orcid.org/0000-0001-7690-8355

Xiaoting Bian − *College of Chemical Engineering, Inner Mongolia Key Laboratory of High-Value Functional Utilization of Low Rank Carbon Resources, Inner Mongolia University of Technology, Hohhot, Inner Mongolia 010051, China*

Xiaojuan Fu − *The Institute of Products Quality Inspection and Research Inner Mongolia, Hohhot, Inner Mongolia 010000, China*

Xue Bai − *College of Chemical Engineering, Inner Mongolia Key Laboratory of High-Value Functional Utilization of Low Rank Carbon Resources, Inner Mongolia University of Technology, Hohhot, Inner Mongolia 010051, China*

Complete contact information is available at:
https://pubs.acs.org/10.1021/acsomega.3c00018

Notes

The authors declare no competing financial interest.

■ REFERENCES

(1) Li, W.; Zhu, Y. M.; Hu, C. Q.; Han, S. B.; Wu, J. S. Hydrocarbon generation and chemical structure evolution from confined pyrolysis of bituminous coal. *ACS Omega* **2020**, *5*, 19682−19694.

(2) Song, Y. M.; Teng, Y. Y.; Li, N.; He, R. X.; Liu, Q. S.; Wang, Y. F. Microstructural evolution during pyrolysis of Shengli lignite and hydrochloric acid-demineralized lignite. *J. Fuel Chem. Technol.* **2021**, *49*, 415−421.

(3) Wang, Y. F.; Song, Y. M.; Zhi, K. D.; Li, Y.; Teng, Y. Y.; He, R. X.; Liu, Q. S. Combustion kinetics of Chinese Shenhua raw coal and its pyrolysis carbocoal. *J. Energy Inst.* **2017**, *90*, 624−633.

(4) Watanabe, W. S.; Zhang, D. K. The effect of inherent and added inorganic matter on low-temperature oxidation reaction of coal. *Fuel Process. Technol.* **2001**, *74*, 145−160.

(5) Li, X.; Li, C. W.; Zhang, H. J.; Li, W. F. Analysis on the status and problems of lignite application in China. *Appl. Chem. Ind.* **2020**, *49*, 1226−1230.

(6) Li, Y.; Zhou, C. L.; Li, N.; Zhi, K. D.; Song, Y. M.; He, R. X.; Teng, Y. Y.; Liu, Q. S. Production of high H_2/CO syngas by steam gasification of Shengli lignite: Catalytic effect of inherent minerals. *Energy Fuels* **2015**, *29*, 4738−4746.

(7) Cheng-hao, H.; Sheng-hua, Z.; Yong-hui, B.; Fan, L. Effect of CO_2 on pyrolysis behavior of Shengli lignite. *J. Fuel Chem. Technol.* **2017**, *45*, 272−278.

(8) Gao, J. S. *Coal pyrolysis of coking and coal tar processing*; Chemical Industry Press: Beijing, 2010.

(9) Qiu, Q. L.; Pan, D. P.; Zeng, F.; Liu, L. L.; Qiu, X. L. Catalytic effect of metal chlorides on coal pyrolysis using TG & PY-GC/MS. *Combust. Sci. Technol.* **2020**, *194*, 2255−2267.

(10) Zhang, K.; Lu, P.; Guo, X. T.; Wang, L. J.; Lv, H. K.; Wang, Z. H.; He, Y. High-temperature pyrolysis behavior of two different rank coals in fixed-bed and drop tube furnace reactors. *J. Energy Inst.* **2020**, *93*, 2271−2279.

(11) Zhang, K.; Li, Y.; wang, Z. H.; Li, Q.; Whiddon, R.; He, Y.; Cen, K. Pyrolysis behavior of a typical Chinese sub-bituminous Zhundong coal from moderate to high temperatures. *Fuel* **2016**, *185*, 701−708.

(12) Xu, F.; Liu, H.; Wang, Q.; Pan, S.; Zhao, D.; Liu, Q.; Liu, Y. ReaxFF-based molecular dynamics simulation of the initial pyrolysis mechanism of lignite. *Fuel Process. Technol.* **2019**, *195*, 106147.

(13) He, X.; Zhu, H. Q.; Huo, Y. J.; Wang, W. Study on the Formation Mechanism of the Pyrolysis Products of Lignite at Different Temperatures Based on ReaxFF-MD. *ACS Omega* **2021**, *6*, 35572−35583.

(14) He, Q. Q.; Wan, K. J.; Hoadley, A.; Yeasmin, H.; Miao, Z. Y. TG−GC−MS study of volatile products from Shengli lignite pyrolysis. *Fuel* **2015**, *156*, 121−128.

(15) Liu, P.; Zhang, D. X.; Wang, L. L.; Zhou, Y.; Pan, T. Y.; Lu, X. L. The structure and pyrolysis product distribution of lignite from different sedimentary environment. *Appl. Energy* **2016**, *163*, 254−262.

(16) Zhou, C. L.; Liu, Q. S.; Li, Y.; Zhi, K. D.; Teng, Y. Y.; Song, Y. M.; He, R. X. Effects of inherent minerals on the production of pyrolysis gases and the corresponding kinetics for Shengli lignite. *Chem. Ind. Eng. Soc. China* **2013**, *33*, 21−27.

(17) Xu, B.; Cao, Q. X.; Kuang, D. Y.; Gasem, K. A. M.; Adidharma, H.; Ding, D.; Fan, M. H. Kinetics and mechanism of CO_2 gasification of coal catalyzed by Na_2CO_3, $FeCO_3$ and Na_2CO_3-$FeCO_3$. *J. Energy Inst.* **2020**, *93*, 922−933.

(18) Kumar, S.; Wang, Z. H.; Kang, Z.; Xia, J.; Whiddon, R.; He, Y.; Gul-e-Rana, J.; Bairq, Z. A. S.; Cen, K. F. Influence of temperature and $Ca(OH)_2$ on releasing tar and coal gas during lignite coal pyrolysis and char gasification. *Chin. J. Chem. Eng.* **2019**, *27*, 2788−2798.

(19) Feng, J.; Xue, X. Y.; Li, X. H.; Li, W. Y.; Guo, X. F.; Liu, K. Products analysis of Shendong long-flame coal hydropyrolysis with iron-based catalysts. *Fuel Process. Technol.* **2015**, *130*, 96−100.

(20) Gong, X. Z.; Guo, Z. C.; Wang, Z. Variation of char structure during anthracite pyrolysis catalyzed by Fe_2O_3 and its influence on char combustion reactivity. *Energy Fuels* **2009**, *23*, 4547−4552.

(21) Wang, Z. H.; Tan, J. X.; He, Y.; Yuan, Y.; Liu, L. L.; Zhu, Y. Q.; Cen, K. F. Catalytic effect of metal chloride additives on the volatile gas release characteristics for high-temperature lignite pyrolysis. *Energy Fuels* **2019**, *33*, 9437−9445.

(22) Xue-jun, Q. I.; Wen-wu, S.; Liang, L. Effect of iron on Shengli brown coal char structure and its influence on gasification reactivity. *J. Fuel Chem. Technol.* **2015**, *43*, 554−559.

(23) Jiang, X. X. Effect of iron catalyst on coal depolymerization. *Coal Technol.* **2018**, *37*, 301−304.

(24) Fu, Y.; Guo, Y. H.; Zhang, K. X. Effect of three different catalysts (KCl, CaO, and Fe_2O_3) on the reactivity and mechanism of low-rank coal pyrolysis. *Energy Fuels* **2016**, *30*, 2428−2433.

(25) Wang, G. H.; Ma, Z. Y.; Wang, Q. D. Effect of metal salts on the decomposition characteristics of Mengdong lignite. *Energy Sources, Part A* **2019**, *42*, 246−257.

(26) Song, Y. M.; Li, Na.; Ban, Y. P.; Teng, Y. Y.; Zhi, K. D.; He, R. X.; Zhou, H. C.; Liu, Q. S. Combustion characteristics and surface morphology of different particle size Shengli lignite. *J. Inn. Mong. Univ. Sci. Technol.* **2017**, *36*, 185−190.

(27) Cheng, X. J.; Shi, L.; Liu, Q. Y.; Liu, Z. Y. Effect of a HF−HF/HCl treatment of 26 coals on their composition and pyrolysis behavior. *Energy Fuels* **2019**, *33*, 2008−2017.

(28) Liu, L. L.; Kumar, S.; Wang, Z. H.; He, Y.; Liu, J. Z.; Cen, K. F. Catalytic effect of metal chlorides on coal pyrolysis and gasification part I. Combined TG-FTIR study for coal pyrolysis. *Thermochim. Acta* **2017**, *655*, 331−336.

(29) Teng, Y. Y.; Bian, X. T.; Song, Y. M.; Wang, B. Z.; Li, N.; He, R. X.; Wang, Y. F.; Liu, Q. S. Effect of the Iron Component on Microcrystalline Structure Evolution of Hydrochloric Acid-Demineralized Lignite during the Pyrolysis Process. *ACS Omega* **2022**, *7*, 29079−29085.

(30) Xie, X.; Zhao, Y.; Qiu, P. H.; Lin, D.; Qian, J.; Hou, H. M.; Pei, J. T. Investigation of the relationship between infrared structure and pyrolysis reactivity of coals with different ranks. *Fuel* **2018**, *216*, 521−530.

(31) Niu, Z. Y.; Liu, G. J.; Yin, H.; Zhou, C. C.; Wu, D.; Yousaf, B.; Wang, C. M. In-situ FTIR study of reaction mechanism and chemical kinetics of a Xundian lignite during non-isothermal low temperature pyrolysis. *Energy CONVERS. Manage.* **2016**, *124*, 180−188.

(32) Xu, Y.; Zhang, Y. F.; Wang, Y.; Zhang, G. J.; Chen, L. Gas evolution characteristics of lignite during low-temperature pyrolysis. *J. Anal. Appl. Pyrolysis* **2013**, *104*, 625−631.

(33) Zhao, B. Q.; Li, N.; Chen, C.; Shi, S. L.; Ban, Y. P.; Song, Y. M.; He, R. X.; Liu, Q. Analysis of structural evolution and gas generation mechanism during the pyrolysis of Shengli lignite. *J. China Coal Soc.* **2019**, *44*, 596−603.

(34) Xie, Y.; Xu, W.; Dong, X.; Cai, L. Study on the structure and pyrolysis reactivity of coal. *Hans J. Chem. Eng. Technol.* **2020**, *10*, 271−282.

(35) Liu, S. Q.; Tuo, K. Y.; Wang, L. P.; Chen, G. Characteristics of catalytic pyrolysis of low-rank coal via microwave-assisted Fe. *J. China Coal Soc.* **2020**, *45*, 1519−1526.

(36) Murakami, K.; Shirato, H.; Ozaki, J.; Nishiyama, Y. Effects of metal ions on the thermal decomposition of brown coal. *Fuel Process. Technol.* **1996**, *46*, 183−194.

(37) Yin-min, S.; Wei, F.; Yun-fei, W.; Na, L.; Yan-peng, B.; Ying-yue, T.; Ke-duan, Z.; Run-xia, H.; Hua-cong, Z.; Quan-sheng, L. Structure characteristics of unreacted residues in combustion of Shengli lignite and effect of Fe components. *J. Fuel Chem. Technol.* **2016**, *44*, 1447−1456.

(38) Xiong, G.; Li, Y. S.; Jin, L. J.; Hu, H. Q. In situ FT-IR spectroscopic studies on thermal decomposition of the weak covalent bonds of brown coal. *J. Anal. Appl. Pyrolysis* **2015**, *115*, 262−267.

(39) Yan, J. C.; Lei, Z. P.; Li, Z. K.; Wang, Z. C.; Ren, S.; Kang, S.; Wang, X.; Shui, H.; Shui, H. F. Molecular structure characterization of low-medium rank coals via XRD, solid state ^{13}C NMR and FTIR spectroscopy. *Fuel* **2020**, *268*, 117038.

(40) Hu, L.; Wei, X. Y.; Zhang, F. B.; Lv, H. P.; Xu, M. L.; Zong, Z. M. Effect of isopropanolysis on the structure variation and pyrolysis behaviors of Wucaiwan lignite. *J. Anal. Appl. Pyrolysis* **2021**, *154*, 105012.

(41) Song, Y.; Feng, W.; Li, N.; Li, Y.; Zhi, K.; Teng, Y.; He, R.; Zhou, H.; Liu, Q. Effects of demineralization on the structure and combustion properties of Shengli lignite. *Fuel* **2016**, *183*, 659−667.